Palladium Catalysts

DOI: 10.1002/anie.201107376

Porous Single-Crystalline Palladium Nanoparticles with High Catalytic Activities**

Feng Wang, Chuanhao Li, Ling-Dong Sun, Chun-Hu Xu, Jianfang Wang,* Jimmy C. Yu, and Chun-Hua Yan**

Catalysis is essential in chemical production, solar energy harvesting, pollution control, and food processing. Industrial metal-based catalysts are usually ultrasmall nanoparticles (NPs) dispersed on supports. Owing to the presence of multiple components and size scales, investigating the dependence of the catalytic performance on the composition, size, and structure is often difficult. In the past 15 years, advances in nanotechnology have enabled the preparation of noble-metal NPs with controllable sizes, facets, and compositions. Applying these NPs for catalysis can not only benefit our understanding of the structure-determined catalytic activity and selectivity, but also help in designing better catalysts.[1–8] For example, judicious control of the preparation conditions can produce metal NPs with different facets.[2,3,6,7] Metal NPs with high-index facets are usually more catalytically active than those with low-index facets. Coating metal NP catalysts with porous silica shells can improve their high-temperature stability.[5] To achieve economical catalysis, catalytic NPs can be integrated with magnetic components, thus allowing easy purification and recycling.[4] Bilayers of metal and oxide NPs can be utilized for tandem reactions.[8]

Furthermore, the catalytic performance of metal NPs can also be improved by control of their morphologies. Many efforts have been devoted to the control of metal NP shapes.[9–11] Dendrites have recently received much attention because they are porous, their branches provide many high-index facets,[12] and they can be readily separated and recycled. In the past few years, pure Pt,[13–18] Pt-on-Pd,[12,19–21] Au/Pd core–Pt shell,[22] and Rh[23] dendritic NPs have been prepared chemically. Dendritic Pt NPs have been shown to be more active in ethylene hydrogenation than Pt cubes and cuboctahedrons.[13] Pt-on-Pd nanodendrites have been found to be 2.5 times more active than C-supported Pt catalysts and 5 times more active than Pt-black catalysts for O_2 reduction.[12] These results suggest that engineering noble metals into porous NPs is an attractive approach for achieving high catalytic performance.

Herein, we describe the facile preparation of porous single-crystalline Pd NPs of controllable sizes. Rapid growth was found to be crucial for their formation. The porous Pd NPs are more catalytically active for the Suzuki coupling reaction than Pd nanospheres and commercial C-supported Pd NPs (Pd/C) at both 85 °C and room temperature. Moreover, they also exhibit remarkable substrate selectivity. We note that there have been no reports on the room-temperature catalytic activities of Pd nanostructures for the Suzuki coupling reaction.

The Pd NP samples were prepared by using a seed-mediated method in aqueous solutions with cetyltrimethylammonium chloride (CTAC) as the stabilizing agent (see the Supporting Information for the experimental details). The sizes of the Pd NPs were relatively uniform, as revealed by transmission electron microscopy (TEM) imaging (Figure 1a). High-angle annular dark-field scanning TEM (HAADF–STEM) imaging shows that the Pd NPs assume a roughly spherical shape and are porous (Figure 1b). N_2-sorption measurements were performed to determine the

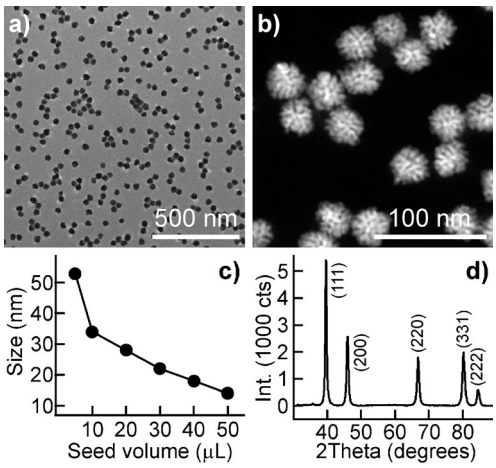

Figure 1. a) TEM and b) HAADF–STEM images of porous Pd NPs with size of 34 nm. c) Plot of the average NP size versus the seed volume. The standard deviation in the size for the largest NP sample is 4 nm, and those for the other smaller NP samples are 1 nm. d) XRD pattern of porous Pd NPs with size of 53 nm.

[*] F. Wang, Prof. L.-D. Sun, C.-H. Xu, Prof. C.-H. Yan
State Key Lab of Rare Earth Materials Chemistry and Applications
Peking University, Beijing 100871 (China)
E-mail: sun@pku.edu.cn
yan@pku.edu.cn
F. Wang, Prof. J. F. Wang
Department of Physics, The Chinese University of Hong Kong
Shatin, Hong Kong SAR (China)
E-mail: jfwang@phy.cuhk.edu.hk
C. H. Li, Prof. J. C. Yu
Department of Chemistry, The Chinese University of Hong Kong
Shatin, Hong Kong SAR (China)

[**] This work was supported by the National Natural Science Foundation of China (Project Code: 20931160429) and the Research Grants Council of Hong Kong (NSFC/RGC Joint Scheme, Ref.: N_CUHK465/09, Project Code: 2900339; Direct Allocation, Project Code: 2060417).

Supporting information for this article is available on the WWW under http://dx.doi.org/10.1002/anie.201107376.

© 2012 Wiley-VCH Verlag GmbH & Co. KGaA, Weinheim

surface areas of the Pd NP samples, but were unsuccessful, owing to the aggregation and coalescence caused by drying during the measurements. The NP sizes, which were obtained by measuring the NP diameter on the TEM images, is readily controlled by varying the seed volume. The average size decreases from 53 to 14 nm as the seed amount is increased (Figure 1c and Figure S1 in the Supporting Information). Figure 1d shows the X-ray diffraction (XRD) pattern of the sample sized at 53 nm. All of the peak positions and intensities accord well with the face-centered-cubic structure of palladium (JCPDS No. 46-1043), indicating high crystallinity. The average grain size estimated using the Scherrer formula from all the peaks is 49 nm. This value is close to the average size obtained from the TEM images, implying that each porous Pd NP might be single-crystalline instead of being composed of randomly oriented small nanocrystals.

We characterized the crystalline structure of the individual NPs with high-resolution (HR) TEM imaging and electron diffraction (ED) (Figure 2). For the large NPs, the HRTEM images recorded at different positions on a single NP show atomic lattices with the same orientation (Figure 2a–c). For the small NPs, the atomic lattice of an entire NP can be observed in one HRTEM image (Figure 2d). In addition, the imaging contrast on the small NPs is non-uniform. The center of the NP shown in Figure 2d is brighter than the exterior. The non-uniform contrast also suggests the porous nature of the single-crystalline NPs. The HRTEM images in Figure 2a–d were taken along the [011] lattice direction. We also observed the atomic lattices of the porous NPs along the [112] lattice direction (Figure S2 in the Supporting Information).

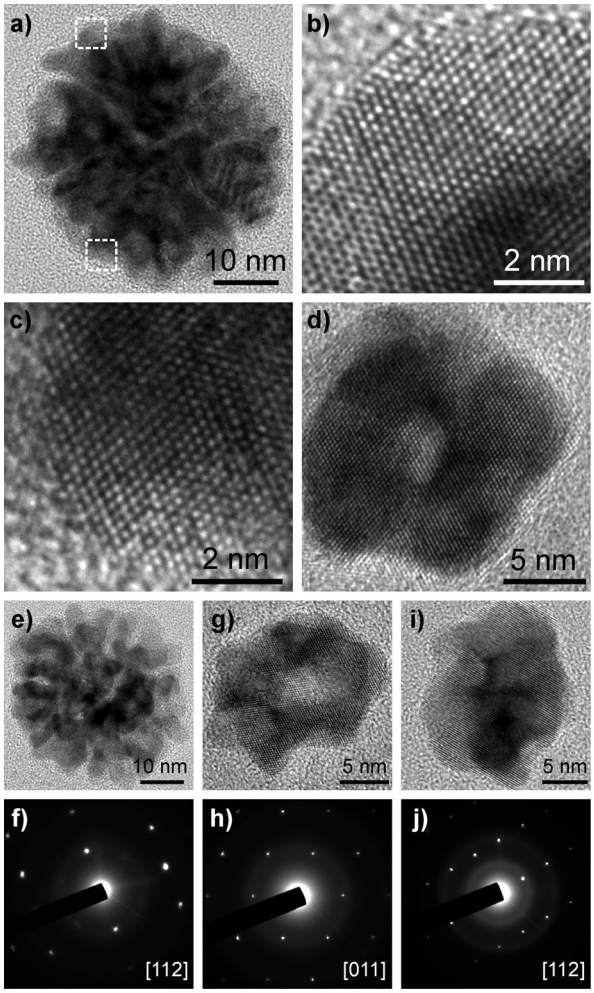

Figure 2. a) TEM image of a single porous Pd NP with size of 53 nm. b,c) HRTEM images recorded from the regions indicated by the upper and lower boxes in (a), respectively. d) HRTEM image of a single porous Pd NP with size of 18 nm. e–j) TEM images and corresponding ED patterns of the porous Pd NPs. The NP in (e,f) is from the sample sized at 53 nm, and those in (g–j) are from the sample sized at 18 nm. The numbers in the ED patterns indicate the zone axes.

ED patterns acquired on the Pd NPs of varying sizes under different lattice orientations all display single sets of sharp diffraction spots (Figure 2e–j). Taken together, the HRTEM imaging and ED results unambiguously corroborate that the porous Pd NPs are single-crystalline. Each Pd NP contains many small domains that are 3–7 nm large and oriented in the same crystalline direction. Moreover, the porous NPs exhibit many atomic steps on their surfaces, as revealed by the HRTEM images. The Pd atoms on these atomic steps can serve as catalytically active sites because of their coordinative unsaturation. We note that there have been only two reports on branched, single-crystalline metal NPs, which are Pt[15] and Pt-on-Pd.[12] In those two studies, the single-crystalline nature is evidenced only by the HRTEM images and Fourier transforms along the [011] direction.

The formation of the porous Pd NPs might undergo two mechanisms. One is the formation of very small Pd nanocrystals and the subsequent oriented integration. The other is seed-mediated growth. Our TEM results strongly support the second mechanism from three aspects. First, no single small Pd nanocrystals are seen under TEM imaging. Second, the sizes of the porous Pd NPs are well controlled by the seed amount. Third, the size distributions of the porous NPs are narrow. To understand better the growth mechanism, we studied their time-dependent morphological evolution by TEM imaging (Figure S3 in the Supporting Information). The major growth step was found to be completed rapidly in the first few seconds after the injection of the reducing agent. The sizes of the products collected subsequently at varying periods of time remain nearly the same. Within 1 min of growth, the number and size of the pores in the NPs are small. More pores are seen with increasing growth periods of time, and their sizes increase. In addition, no small Pd nanocrystals were observed. This evolution suggests that the porous NPs are produced through direct homoepitaxial growth on the Pd seeds.

We performed additional control experiments to unravel the growth mechanism further. First, cetyltrimethylammonium bromide (CTAB) was used for the growth (Figure S4 in the Supporting Information). Second, the growth was carried out in a mixture of CTAC and CTAB at varying molar ratios (Figure S5 in the Supporting Information). Third, an excess amount of halide anions (F^-, Cl^-, and Br^-) was introduced in the growth solution in addition to CTAC or CTAB (Figure S6 in the Supporting Information). The binding of ammonium surfactants to noble metals is assisted by the adsorption of

 © 2012 Wiley-VCH Verlag GmbH & Co. KGaA, Weinheim

halide anions to the metal surface.[24] The binding strengths of halide ions to the Pd surface increase in the order of F^-, Cl^-, and Br^-. Porous Pd NPs are obtained only from the growth with F^- and CTAC. When Br^- ions are present or the concentration of Cl^- is very high, the growth is much slower and produces solid Pd NPs. Fourth, the growth solution pH was adjusted from 1–12 (Figure S7 in the Supporting Information). A distinct morphological transition occurs in the pH range 6.5–7.5, where the products change from solid NPs into porous ones. In addition, the growth becomes faster as the pH value is raised. The fast growth and morphological change is ascribed to the fact that the reducing capability of the reducing agent, ascorbic acid, increases with the solution pH value.

The above results suggest that rapid growth is essential for the formation of the porous single-crystalline Pd NPs (Figure 3). It produces Pd NPs with many small crevices.

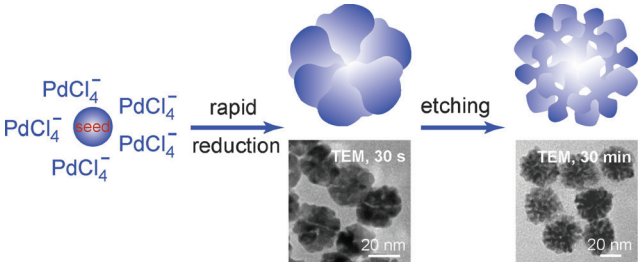

Figure 3. Schematic illustration of the proposed growth mechanism of the porous single-crystalline Pd NPs. The TEM images show the products obtained after growth for 30 s and 30 min, respectively. The volume of the seed solution was 0.010 mL.

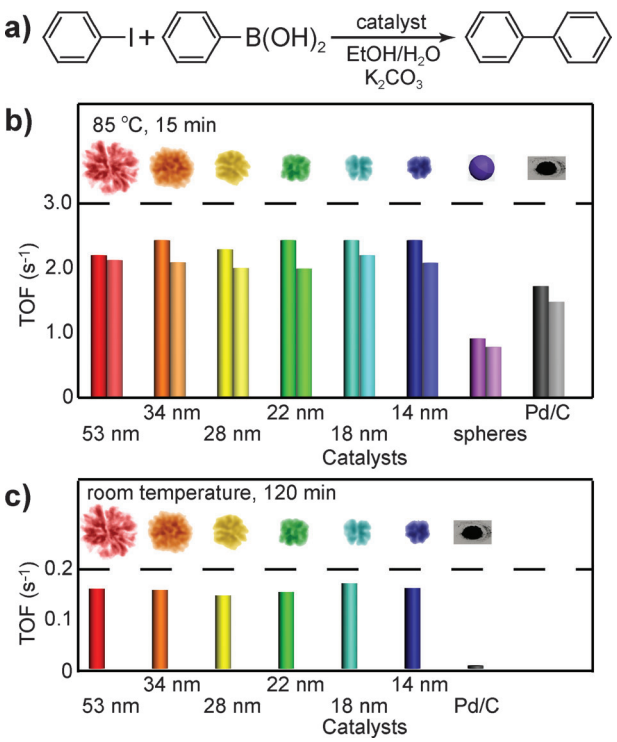

Figure 4. TOF values of the Pd-based catalysts for the coupling between iodobenzene and phenylboronic acid. a) Reaction equation. b) TOF values at 85 °C for 15 min. For each catalyst, the left column shows the TOF value in the first run, and the right one indicates the TOF value in the second run. c) TOF values at room temperature for 120 min.

The initially formed Pd NPs then undergo oxidation owing to the presence of Cl^- and O_2 in the solution.[25] The oxidative etching occurs preferentially at the highly active sites in the crevices, giving the porous structure. If the growth is slow, solid NPs will be produced. Pores are difficult to form in these solid NPs through the oxidative etching.

We tested the catalytic activities of the porous Pd NPs with the Suzuki coupling reaction, a widely used model reaction. The amounts of Pd contained in the catalysts were adjusted to be the same by inductively coupled plasma atomic emission spectroscopy (ICP–AES) (Table S1 in the Supporting Information). The turnover frequencies (TOFs) were calculated according to the total amounts of Pd. For the coupling reaction between phenylboronic acid and iodobenzene (Figure 4a) at 85 °C, the reaction yields of biphenyl range from 89 to 99 % for the differently sized porous Pd NPs (Table S2 in the Supporting Information). The TOF values are around 2.5 s^{-1} (Figure 4b). The size-independence of the catalytic activity arises from the porous nature of these NPs, which makes the NPs have approximately the same specific surface area. In comparison, the TOF values are 0.92 and 1.75 s^{-1} for a Pd nanosphere sample with a size of 24 ± 2 nm (Figure S8 in the Supporting Information) and the commercial Pd/C containing less-than-5-nm Pd NPs, respectively. The TOFs of the porous Pd NPs are approximately 3 and 1.5 times those of the Pd nanospheres and Pd/C. Moreover, the catalytic efficiencies of the porous Pd NPs are much higher than those reported for Pd nanospheres,[26] nanorods,[27] nanobranches,[27] and icosahedrons[28] in terms of the Pd amount and reaction time. In those studies, the molar percentages of Pd relative to iodobenzene are 3.0 %, 1.6 %, 1.8 %, and 1.7 %, respectively. The reaction time ranges from 4 to 8 h. The reaction yields are around 90 %. In our experiments, the molar percentage of Pd relative to iodobenzene is 0.04 %, and the reaction time is only 15 min.

The recycling capability of the porous Pd NPs was examined by removing the supernatant after the reaction and leaving the precipitated Pd NPs for another run of the reaction. Product yields above 80 % were obtained in the second run (Figure 4b and Table S3 in the Supporting Information). The morphologies of the Pd NPs remain nearly unchanged after the first run (Figure S9 in the Supporting Information). In addition, reaction yields of 80–90 % were obtained in the first four cycles for the 53-nm- and 18-nm-sized Pd NP samples (Table S4 in the Supporting Information). The reaction yields dropped to 10.0 % at the fifth cycle, as a result of aggregation of the Pd NPs at the bottom of the reaction flask. To avoid aggregation, we further deposited the 53-nm-sized Pd NPs on a piece of cotton fabric with a size of 2 cm × 2 cm and immersed it in the solution for catalyzing the coupling reaction between iodobenzene and phenylboronic acid. The reaction was carried out at 85 °C for 30 min. The reaction yields of biphenyl were above 80 % even

© 2012 Wiley-VCH Verlag GmbH & Co. KGaA, Weinheim

after 11 cycles (Figure S10 and Table S5 in the Supporting Information). We are currently carrying out more catalytic studies by depositing various metal nanostructures on different types of fabrics. The amounts of the leached Pd were measured with ICP-AES to be 1.0–1.5% after the reaction mixture containing the 34-nm-sized Pd NPs was kept at 85°C for 15 min. The leached Pd was found to show no catalytic activity under our reaction conditions.

The TOF values of the vaiously sized Pd NPs at room temperature were 0.16 s^{-1}, which is 30 times that of the Pd/C (Figure 4c and Table S6 in the Supporting Information). When bromobenzene, which is less reactive than iodobenzene because of the larger C–Br bond energy, is used, the TOF values of the 34-nm-sized Pd NP sample were 0.24 s^{-1} at 85°C and 39.3 h^{-1} at room temperature. Both of these values are around 6 times those of the Pd/C (Table S7 in the Supporting Information). So far, the Suzuki coupling reactions at room temperature have been reported only with Pd complexes as the catalysts.[29,30] There have been no reports with Pd nanostructures as the catalysts at room temperature.

To help in understanding the higher catalytic activities of the porous Pd NPs than that of the Pd/C, we measured the cyclic voltammetry (CV) curves for O-atom sorption on three Pd NP samples and the Pd/C (Figure S11 in the Supporting Information). The average electrochemical surface areas obtained from O atom sorption were (5.1 ± 0.1), (5.7 ± 0.4), (5.6 ± 0.6), and $(13.3 \pm 0.7) \times 10^4$ $cm^2 g^{-1}$ for the 34-nm-, 28-nm-, 18-nm-sized Pd NP samples, and the Pd/C, respectively (Table S8 in the Supporting Information). The average electrochemical surface areas of the three differently sized Pd NP samples are very similar, indicating that the differently sized Pd NPs have approximately the same specific surface area. Although the electrochemical surface area of the Pd/C is larger than those of the porous Pd NC samples, the Pd NP samples exhibit higher TOF values. This behavior might be caused by the different adsorption abilities of the species involved in the catalytic reaction and electrochemical measurement.

Finally, we investigated the catalytic activities of the 34-nm-sized Pd NPs for the reactions between the respective position isomers of bromoanisole and tolylboronic acid. A total of nine reactions were performed. At 85°C, all of the reactions involving *m*-bromoanisole show relatively high TOF values (Figure S12 and Tables S9 and S10 in the Supporting Information). The reactions involving *o*-tolylboronic acid are less efficient than those involving *m*- and *p*-tolylboronic acid. The TOF value of the reaction between *o*-bromoanisole and *m*-tolylboronic acid is the highest. In comparison, the average TOF value at room temperature is about 1/20 of that at 85°C. The overall trend in the TOFs is also different from that at 85°C. These results indicate that the porous Pd NPs are also highly active for the reactions involving complicated molecules. More studies will be needed to compare the substrate selectivities between the porous Pd NPs and Pd complexes and better understand the catalytic properties of the porous Pd NPs. However, we also tested the catalytic activities of the 34-nm-sized Pd NPs for the reaction between chlorobenzene and phenylboronic acid both at 85°C and room temperature. No reaction activities were obtained.

In summary, we have shown the size-controlled growth of porous single-crystalline Pd NPs. The formation of the porous Pd NPs is ascribed to a rapid-growth process. The porous Pd NPs display high catalytic activities toward the Suzuki coupling reaction at both raised and room temperatures. The TOF values of the porous Pd NPs are around 30 times that of the commercial Pd/C for iodobenzene, and 6 times for bromobenzene. The Pd NPs also exhibit good substrate selectivity. The high catalytic activities of the porous Pd NPs is attributed to their large surface area and high concentration of coordinatively unsaturated surface atoms. Our results demonstrate that porous metal NPs could provide an excellent catalytic platform for organic reactions.

Received: October 19, 2011
Revised: March 9, 2012
Published online: April 3, 2012

Keywords: C–C coupling · crystal growth · mesoporous materials · nanoparticles · palladium

[1] K. M. Bratlie, H. Lee, K. Komvopoulos, P. D. Yang, G. A. Somorjai, *Nano Lett.* **2007**, *7*, 3097–3101.
[2] N. Tian, Z.-Y. Zhou, S.-G. Sun, Y. Ding, Z. L. Wang, *Science* **2007**, *316*, 732–735.
[3] Y. Y. Ma, Q. Kuang, Z. Y. Jiang, Z. X. Xie, R. B. Huang, L. S. Zheng, *Angew. Chem.* **2008**, *120*, 9033–9036; *Angew. Chem. Int. Ed.* **2008**, *47*, 8901–8904.
[4] J. P. Ge, T. Huynh, Y. X. Hu, Y. D. Yin, *Nano Lett.* **2008**, *8*, 931–934.
[5] S. H. Joo, J. Y. Park, C.-K. Tsung, Y. Yamada, P. D. Yang, G. A. Somorjai, *Nat. Mater.* **2009**, *8*, 126–131.
[6] C.-L. Lu, K. S. Prasad, H.-L. Wu, J. A. Ho, M. H. Huang, *J. Am. Chem. Soc.* **2010**, *132*, 14546–14553.
[7] F. Wang, C. H. Li, L.-D. Sun, H. S. Wu, T. Ming, J. F. Wang, J. C. Yu, C.-H. Yan, *J. Am. Chem. Soc.* **2011**, *133*, 1106–1111.
[8] Y. Yamada, C.-K. Tsung, W. Y. Huang, Z. Y. Huo, S. E. Habas, T. Soejima, C. E. Aliaga, G. A. Somorjai, P. D. Yang, *Nat. Chem.* **2011**, *3*, 372–376.
[9] A. R. Tao, S. Habas, P. D. Yang, *Small* **2008**, *4*, 310–325.
[10] Y. N. Xia, Y. J. Xiong, B. Lim, S. E. Skrabalak, *Angew. Chem.* **2009**, *121*, 62–108; *Angew. Chem. Int. Ed.* **2009**, *48*, 60–103.
[11] D. S. Wang, Y. D. Li, *Adv. Mater.* **2011**, *23*, 1044–1060.
[12] B. Lim, M. J. Jiang, P. H. C. Camargo, E. C. Cho, J. Tao, X. M. Lu, Y. M. Zhu, Y. N. Xia, *Science* **2009**, *324*, 1302–1305.
[13] H. Lee, S. E. Habas, S. Kweskin, D. Butcher, G. A. Somorjai, P. D. Yang, *Angew. Chem.* **2006**, *118*, 7988–7992; *Angew. Chem. Int. Ed.* **2006**, *45*, 7824–7828.
[14] X. W. Teng, X. Y. Liang, S. Maksimuk, H. Yang, *Small* **2006**, *2*, 249–253.
[15] M. A. Mahmoud, C. E. Tabor, M. A. El-Sayed, Y. Ding, Z. L. Wang, *J. Am. Chem. Soc.* **2008**, *130*, 4590–4591.
[16] L. Wang, Y. Yamauchi, *J. Am. Chem. Soc.* **2009**, *131*, 9152–9153.
[17] A. Mohanty, N. Garg, R. C. Jin, *Angew. Chem.* **2010**, *122*, 5082–5086; *Angew. Chem. Int. Ed.* **2010**, *49*, 4962–4966.
[18] S. H. Sun, G. X. Zhang, D. S. Geng, Y. G. Chen, R. Y. Li, M. Cai, X. L. Sun, *Angew. Chem.* **2011**, *123*, 442–446; *Angew. Chem. Int. Ed.* **2011**, *50*, 422–426.
[19] Z. M. Peng, H. Yang, *J. Am. Chem. Soc.* **2009**, *131*, 7542–7543.
[20] B. Lim, Y. N. Xia, *Angew. Chem.* **2011**, *123*, 78–87; *Angew. Chem. Int. Ed.* **2011**, *50*, 76–85.
[21] L. Wang, Y. Nemoto, Y. Yamauchi, *J. Am. Chem. Soc.* **2011**, *133*, 9674–9677.

 © 2012 Wiley-VCH Verlag GmbH & Co. KGaA, Weinheim

[22] L. Wang, Y. Yamauchi, *J. Am. Chem. Soc.* **2010**, *132*, 13636 – 13638.
[23] H. Zhang, W. Y. Li, M. S. Jin, J. Zeng, T. Yu, D. R. Yang, Y. N. Xia, *Nano Lett.* **2011**, *11*, 898 – 903.
[24] H. A. Keul, M. Möller, M. R. Bockstaller, *Langmuir* **2007**, *23*, 10307 – 10315.
[25] B. Lim, M. J. Jiang, J. Tao, P. H. C. Camargo, Y. M. Zhu, Y. N. Xia, *Adv. Funct. Mater.* **2009**, *19*, 189 – 200.
[26] S.-W. Kim, M. Kim, W. Y. Lee, T. Hyeon, *J. Am. Chem. Soc.* **2002**, *124*, 7642 – 7643.
[27] Y.-H. Chen, H.-H. Hung, M. H. Huang, *J. Am. Chem. Soc.* **2009**, *131*, 9114 – 9121.
[28] C. C. Li, R. Sato, M. Kanehara, H. B. Zeng, Y. Bando, T. Teranishi, *Angew. Chem.* **2009**, *121*, 7015 – 7019; *Angew. Chem. Int. Ed.* **2009**, *48*, 6883 – 6887.
[29] B. Saito, G. C. Fu, *J. Am. Chem. Soc.* **2007**, *129*, 9602 – 9603.
[30] T. Nishikata, A. R. Abela, S. L. Huang, B. H. Lipshutz, *J. Am. Chem. Soc.* **2010**, *132*, 4978 – 4979.

 © 2012 Wiley-VCH Verlag GmbH & Co. KGaA, Weinheim